# RADAR ALTIMETRY

# ALTIMETRY, RADAR

Satellite-based radar altimetry over the world's oceans is the main theme of this article. Rather than measure the unknown clearance of the radar above potentially hazardous topography (which is one rationale for an aircraft radar altimeter for example), satellite-based altimeters are designed to measure the height of the ocean's surface relative to an objective reference such as the Earth's mean ellipsoid. Such sea surface height measurements have become essential for a wide variety of applications in oceanography, geodesy, geophysics, and climatology [1]. A satellite-based altimeter circles the Earth in about 90 minutes, generating surface height measurements along its nadir track. These measurements accumulate, providing unique synoptic data that have revolutionized our knowledge and understanding of both global and local phenomena, from El Niño to bathymetry. A satellite-based radar altimeter also provides measurements of significant wave height and wind speed along its nadir track.

Although one might view these altimeters as relatively simple instruments, their phenomenal measurement accuracy and precision requires elegant microwave implementation and innovative signal processing. This article provides an overview of the applications that drive these requirements, and a description of the resulting state-of-the-art design concepts.

A nadir-viewing altimeter in a repeat-track orbit is constrained by a fundamental trade-off between temporal coverage (revisit period $D$ days) and spatial coverage (track separation at the equator $W$ kilometers): $DW$ = constant for a given inclination and altitude. If more than one altimeter is under consideration, either as independent assets or as a pre-planned constellation, then the space/time trade-space is enlarged, and more measurement objectives may be satisfied. The limitations imposed by this constrain have motivated "multi-beam" or "wide swath" altimeter concepts, although all such architectures imply a compromise on height measurement accuracy. The leading example of this genre is reviewed at the end of this article.

The sea surface height (SSH) measurement objectives of space-based altimeters can be grouped into three broad categories: large-scale dynamic sea surface topography, mesoscale oceanic features, and the cryosphere – near-polar sea ice and continental ice sheets. Satellite altimeters dedicated to determining the ocean's large scale dynamic surface topography are characterized by absolute sea surface height measurement accuracy on the order of centimeters along tracks of more than 1000 km, and orbits that retrace their surface tracks every 10 to 20 days. In contrast, mesoscale missions focus on sea surface height signals of less than ∼300 km in length. This application requires measurement precision sufficient to sustain relative height measurements, and for geodetic data, relatively dense track-to-track spacing. Geosat is the leading example of this category, for both geodetic (non-repeat) and mesoscale (exact-repeat) orbits. Observation of oceanic and polar ice sheets requires that the altimeter have robust range and spatial resolution, accuracy, and precision in response to the non-zero average surface slope in both the along-track and cross-track direction of the continental glaciers. Suitable orbits must have near-polar inclination, and multi-year relative accuracy. CryoSat is reviewed as the first example of this class of radar altimeter mission.

Radar altimeters must provide accurate and precise SSH measurements from a spacecraft whose roll and pitch attitudes are not known exactly. These requirements can be satisfied by the pulse-limited altimeter paradigm, which is characterized by (1) large time-bandwidth pulse modulation, (2) antenna directivity that illuminates a surface area larger than the spatially-resolved footprint, and (3) extensive non-coherent (post-detection) waveform averaging. The design of the TOPEX altimeter is described as an example. Footprint resolution and measurement precision can be improved by combining coherent and increased incoherent processing, exemplified by the delay-Doppler altimeter, which borrows applicable techniques from synthetic aperture radar (SAR). The article closes with an overview of future developments and advanced mission concepts.

## RADAR ALTIMETER SATELLITES

All satellite radar altimeters to date (Table 1) are incoherent pulse-limited instruments, as described in a later passage. Since 1973 height measurement accuracy has improved, due primarily to dedicated effort and increasing skill applied to estimation and correction of systematic errors. Performance also has benefitted from improved onboard hardware and algorithms, and improved orbit determination. The Jason-1 altimeter represents the state-of-the-art in absolute sea surface height measurement accuracy (as of the year 2006). On-line access to descriptions of most of these radar altimeter missions may be found at [2].

### Orbits

An altimeter's SSH accuracy on large scales depends to first order on how well the height of the altimeter itself can be determined. Given the state-of-the-art in satellite tracking systems, the dominant error in satellite (radial) position determination is uncertainty in knowledge of the gravity field (often expressed in term of geoid height) [3]. At lower orbit altitudes, the higher-frequency components of the gravity field are enhanced. The impact can be significant. For example, gravity variations of about 400 km wavelength are 100 times larger at an altitude of 500 km than they are at 1000 km. In general, the accuracy of precision orbit determination is better for higher altitudes.

Atmospheric drag is approximately ten times larger at 800 km than at 1200 km [4]. For example, over one orbit at 1200 km altitude, drag imposes a 1-cm decay on the orbit radius. At 800 km altitude, the effect is ten times larger, resulting in a 10-cm decay per orbit. Atmospheric drag increases significantly during periods of higher solar flare activity, the peaks of which occur approximately every eleven years.

Table 1. Summary of Satellite Radar Altimeters

| Altimeter | AgencyYearOrbitInclination Repeat (days)(degrees) | Altitude (km) | Equatorial Spacing (km) | Band | Propagation Measurements | Accuracy |
|---|---|---|---|---|---|---|
| Skylab (3) | NASA1973No∼48 | 435 | – | Ku | None | 50 m |
| GEOS-3 | NASA1975–8No115 | 845 | ∼60 | Ku | None | 50 cm |
| Seasat | NASA1978∼17,3108 | 800 | 160, 800 | Ku | $H_2O$ | 20 cm |
| Geosat | USN1985–9∼3, 17.05108 | 800 | ∼4, 160 | Ku | None | 10 cm |
| ERS-1 | ESA1991–73, 35, 17698.5 | 785 | 20 – 800 | Ku | $H_2O$ | 7 cm |
| TOPEX[1] | NASA1992 –9.91666 | 1336 | 315 | C, Ku | $H_2O$, $e^-$ | 2 cm |
| Poseidon[1] | CNES1992 –9.91666 | 1336 | 315 | Ku | $H_2O$ | 5 cm |
| ERS-2 | ESA1995 –3598.5 | 781 | 80 | Ku | $H_2O$ | 7 cm |
| GFO | USN1998 –17.05108 | 800 | 160 | Ku | $H_2O$ | 5 cm |
| RA-2 | ESA2002 –3598.5 | 800 | 80 | S, Ku | $H_2O$, $e^-$ | 7 cm |
| Jason-1 | CNES2001 –9.91666 | 1336 | 315 | C, Ku | $H_2O$, $e^-$ | 1.5 cm |
| Jason-2 | CNES(2008)9.91666 | 1336 | 315 | C, Ku | $H_2O$, $e^-$ | (1.5 cm) |
| CryoSat | ESA(2009)36992 | 720 | – | Ku | None | (5 cm) |

Whereas a 10-cm decay in radius per orbit may not seem like much for a satellite at 800 km altitude, these decreases accumulate. Smaller orbit radii induce higher spacecraft velocities. Thus, orbit decay accelerates the satellite, shifting its ground track away from its exact repeat path. An altimeter's repeat pattern can be maintained only by replacing the energy removed by drag forces. Active intervention is required, usually in the form of thruster firings of controlled strength, duration, and direction. Orbit maintenance maneuvers are required more frequently when the altimeter's orbit is subject to larger perturbations.

## Review of Missions

The first satellite radar altimeter was the proof-of-concept S-193 instrument (General Electric) that flew on three Skylab missions. The objectives were: to verify predicted waveform response to wind and waves, to measure the radar cross section of the sea at vertical incidence, to measure inter-pulse correlation properties, and to observe the effect of off-nadir antenna orientation. Geos-3 (General Electric) provided the first geodetic and geophysical results of significance within the National Geodetic Satellite Program, including the first maps of sea level variability and the marine geoid. Geos-3 and the S-193 altimeters used conventional pulse compression techniques.

The Seasat altimeter (Johns Hopkins University Applied Physics Laboratory) was the first to use full deramp pulse compression, which opened the way for the very small range resolution required for many oceanographic applications. The deramp technique (described below) has been adopted by all radar altimeters since then. Seasat was designed to measure global ocean topography and the marine geoid, as well as wave height and surface wind speed. The Geosat (Johns Hopkins University Applied Physics Laboratory) altimeter's design was patterned closely after that of the Seasat altimeter. Geosat was a U. S. Navy military satellite whose primary mission was to map the Earth's marine geoid to then-unprecedented accuracy (drifting orbit). Since their declassification in 1995, data from the first 18 month geodetic mission have become the backbone of the global bathymetric chart that is the industry standard [5, 6]. Geosat's secondary mission was to observe dynamic oceanographic phenomena, for which it was maneuvered into an exact repeat orbit (period 17.05 days) [7]. The Geosat Follow-On (GFO) altimeter (E-Systems) is meant to replicate as much as possible the Geosat exact repeat mission, leading towards an operational capability for the U. S. Navy. There has been no dedicated geodetic radar altimeter mission since Geosat, although a new mission known as Abyss-Lite is being actively promoted.

In the late 1980s, planning for satellite radar altimeter missions split into two themes, determined by the relative priority of their measurements. If the altimeter is the prime payload instrument, then the orbit and mission design can be optimized accordingly. This theme was initiated by TOPEX/Poseidon (T/P), a joint United States (NASA) and French (CNES) mission. TOPEX (Johns Hopkins University Applied Physics Laboratory) was designed to measure and map the dynamic ocean topography with sufficient accuracy to determine large-scale circulation patterns [1]. TOPEX' most famous contribution is early observation and near-real-time monitoring of El Niño events, whose height signature over the equatorial eastern Pacific ocean typically is an increase on the order of 10-20 cm with respect to the mean. Poseidon (Alcatel Espace), contributed by France, is a small proof-of-concept instrument that has a solid-state transmitter. Poseidon is the precursor of the Jason altimeters, and the SIRAL instrument aboard CryoSat. Cryosat (described below) will be the first radar altimeter designed to observe polar and continental ice sheets from space.

The T/P orbit repeat period (9.916 days) was chosen carefully to satisfy adequate observation of the dominant aliased tidal constituents. All solar tidal constituents would be ambiguous with other height signals if the repeat period were an integral number of days (20). For T/P, the time of day for each subsequent observation slips by about two hours. The T/P repeat pass footprint location accuracy is better than $\pm$ 1 km, a requirement that is bounded by the cross-track gradient of the oceanic geoid. The T/P instrument package includes a three-frequency radiometer to measure and compensate for propagation delays due to atmospheric moisture ($H_2O$). TOPEX is the first altimeter to use two frequencies to estimate and compensate for propagation delays imposed by ionospheric electrons (*e*-). The Jason-1 altimeter (Alcatel Espace) [8] is designed to follow in the footsteps of TOPEX, figuratively and literally. Following the launch of Jason-1 into the T/P orbit, TOPEX

was maneuvered into a "tandem" phasing so that the measurements of the two altimeters could be cross-calibrated. The follow-on mission Jason-2 will be identical to Jason-1, and may also include an experimental wide swath ocean altimeter (outlined in the closing sections of this article).

If the altimeter is not the primary payload, then the resulting mission and orbit are likely to be determined by other requirements, which may compromise altimetry. The European Space Agency's satellite altimeters (Selenia Spazio) on ERS-1 and ERS-2, as well as the advanced radar altimeter RA-2 [9] (Alenia Spazio) on ESA's Envisat, are of second priority with respect to the other instruments on their respective spacecraft. Their sun-synchronous orbits are less than optimum for precision altimetry. The orbit of ERS-1 was adjusted during its mission to a long repeat period (176 days). That long repeat-period generated a relatively dense surface sampling grid useful for estimating sea ice cover, geodesy, and bathymetry, but is less than optimum for most other applications.

## GLOBAL DYNAMIC TOPOGRAPHY-ACCURACY

The principal objective of an oceanographic satellite radar altimeter designed to observe the dynamic sea surface topography over very large spatial scales is to measure the absolute height $h_s$ of the sea surface (Fig. 1) with respect to the standard reference ellipsoid. The key word here is accuracy: the mean bias error of the measurements with respect to an absolute reference. Height measurement accuracy depends, among other factors, upon the accuracy of accounting for variations in the speed of microwave propagation between the radar and the surface. The absolute SSH measurement problem is challenging because the geophysical signal is small, at most on the order of tens of centimeters, yet that signal has to be derived from a satellite altimeter at altitude of 1400 km or so, whose raw range measurement is subject to corrections as large as several tens of meters, and corrections for the geoid of many tens of meters. The accuracy of estimating the dynamic topographic signal is limited by the corrections for variations in the speed of light (nominally $c$) and other perturbations, as well as the height accuracies of the orbit, marine geoid, tides, and atmospheric pressure. The implied errors have been reduced over the years, after considerable focused effort. State-of-the-art height accuracy (Jason-1) is better than 3 cm (10 day average) or 1.5 cm (1 month average computed with multi-orbit crossover data), which is a remarkable achievement.

The mean sea level, governed primarily by the marine geoid, differs from the reference ellipsoid by $\pm$ 50 m or more, approaching +100 m in parts of the Indian Sea. Often, the geophysical signal of interest is the dynamic topography $\xi$, defined as the distance between the marine geoid $h_G$ and the physical sea surface, corrected for systematic offsets due to tides and atmospheric pressure, for example. The dynamic topography would be zero if the sea were at rest relative to the Earth. The dynamic topography reflects small surface slopes associated with geostrophic currents, of which the Gulf Stream is a well-known example. Cross-stream surface slopes are proportional to the mean current

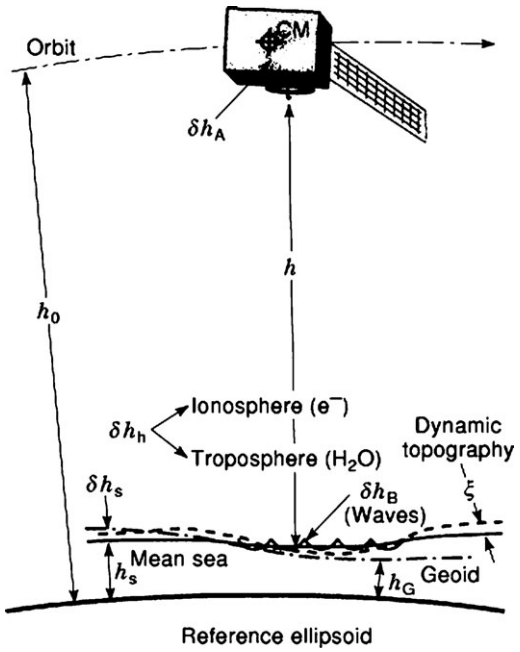


**Figure 1.** A satellite-borne radar altimeter measures the round trip time delay of transmitted signals, from which is deduced the altimetric height $h$ between the satellite's orbit and the reflecting surface. For most geophysical interpretations, the altimetric height is converted to the surface's height, which is described using the standard ellipsoid of the Earth as the reference.

flow rate; the resulting slope signals are indicative of large-scale oceanic circulation patterns.

### The altimeter's measurements

Whereas the objective is determination of the distance between the radar and the sea surface, the altimeter actually measures round-trip delay $t_T$. The altimeter's relative height $h$ is derived from the measured time delay by $h = t_T c/2$, where $c$ is the speed of light. At the accuracy required of an oceanographic altimeter, this deceptively simple proportionality must take into account the small but significant retardation of the radar's microwaves as they propagate through the atmosphere and the ionosphere.

In addition to sea surface height, the satellite radar altimeter's waveform supports two other oceanographic measurements: significant wave height (SWH), and surface wind speed (WS). Over a quasi-flat sea, a pulse-limited altimeter's idealized mean waveform is a step function, whose rise time is equal to the compressed pulse length, and whose position on the time-delay axis is determined by the altimeter's height (Fig. 2). If the sea surface is modulated by gravity waves, the altimetric depth of the surface increases, which reduces the slope of the waveform's leading edge. Hence, SWH is proportional to the waveform rise time. If the sea surface is under stress from wind, the resulting fine-scale roughness decreases the power of the pulse reflected back to the altimeter. Hence, WS is inversely related to mean waveform power. In practice, the inflections of the idealized flat-surface response function waveform are softened by the pulse weighting, and the waveform plateau is attenuated over time by the weighting of

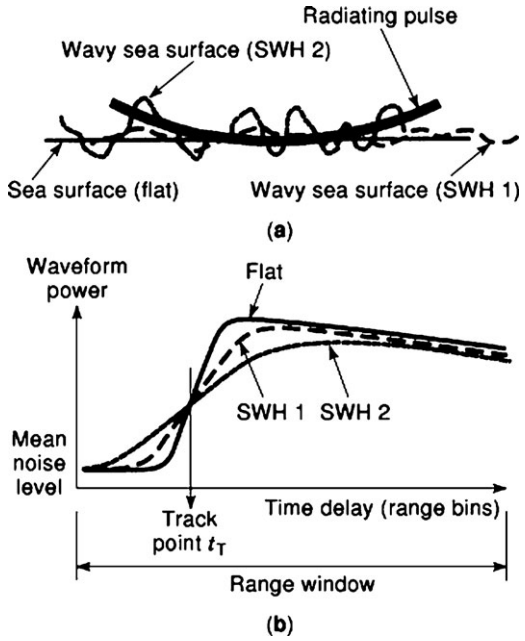


**Figure 2.** A pulse-limited altimeter's radiated signal intersects the wavy surface of the ocean from above (a). The output (averaged) waveform is the altimeter's response to the surface (b). Waveform (round-trip) time delay $t_T$ and leading edge slope indicate height above the surface and the large scale roughness (SWH) of the surface, respectively.

the antenna pattern.

To extract SWH and WS from waveform data, finely tuned algorithms have been developed and validated against *in situ* buoy measurements. For example, the TOPEX Ku-band altimeter measures SWH to within $\pm$ 0.5 m up to more than 5.0 m, and WS within $\pm$1.5 m/s up to more than 15 m/s. These figures correspond to averages over 1 second, or about 6 km along the sub-satellite path of the altimeter's footprint, which typically is 3 km–5 km wide, determined by mean sea state.

## Height Error budget

The ultimate accuracy of an altimeter depends critically on estimation and removal of the systematic errors inherent to the measurement. Once recovered from the altimetry data, sea surface height $h_S$ is used to derive the signal $\xi$ of the dynamic sea surface topography by

$$\xi = h_S - h_G - \delta h_S$$

in which the independent variables imply geophysical corrections: geoid determination ($h_G$) and Earth tides, oceanic tides, inverse barometer corrections, etc ($\delta h_S$).

An oceanographic altimeter collects radar ranging data that are reduced to sea surface height $h_S$ according to

$$h_S = h_O - h - \delta h_A - \delta h_B - \delta h_h \quad (1)$$

where the last three terms on the right hand side of Eq. (2) entail corrections to be derived from electromagnetic (EM) reflection and propagation phenomena. Orbit radial height ($h_O$) is determined through extensive instrumentation and analysis, with a net uncertainty. The magnitude of the uncorrected height errors, and the TOPEX post-compensation residual height uncertainties that remain in $h_S$, are summarized in Table 2.

*Instrument corrections* $\delta h_A$ Height errors that arise in the altimeter and spacecraft environment may be driven close to zero by careful design and calibration [10, 11]. Range delay has to be adjusted to account for the electronic distance from the antenna phase center, through the transmitter, receiver and processor, to the satellite's center of mass. The required timing correction is a function of spacecraft attitude, temperature, and age, among other perturbations. The waveform leading edge delay is tracked dynamically on-board, but not perfectly. After calibration and compensation, the combined equivalent distance root-sum-squared (RSS) uncertainty of TOPEX from all on-board sources is about 3.7 cm, less than two Ku-band wavelengths.

*Surface corrections* $\delta h_B$ The radiated wave front impinges on the sea surface, and then is reflected. In the presence of waves, the mean EM surface sensed by the reflection deviates from the physical sea surface. The resulting height measurement bias occurs because ocean waves tend to reflect more strongly from their troughs than from their crests. Ocean waves also tend to be asymmetrical in their height distribution, described by skewness. This causes the area of the reflecting surface that lies above the mean sea level to be larger than the area below. If scattering were simply proportional to area, this skewness would bias the height measurement. Both EM bias and skewness bias are reduced through empirically derived algorithms that depend on the local significant wave height.

*Propagation corrections* $\delta h_h$ EM propagation is retarded by free electrons in the ionosphere, by the air mass of the troposphere, and by the water content of the troposphere. If uncorrected, the height measurement error from these three sources would be about 2.5 m, intolerable for oceanic radar altimetry. The largest error is due to the dry troposphere, but this contribution varies slowly over the planet, and is not problematic. It can be removed almost completely through application of standard models that depend simply on atmospheric pressure and Earth latitude.

Atmospheric water content may vary considerably with location. The resulting path length changes, if uncorrected, could imply the presence of large but false oceanic height signals. The only reliable way to counteract its effect is to measure the water content directly along the altimeter's propagation path. Atmospheric water content may be estimated rather well with radiometric techniques. TOPEX carries a three-frequency (18 GHz, 21 GHz, and 37 GHz) water vapor radiometer (WVR) whose data are used to reduce the wet troposphere path length error to 1.2 cm [12].

The altimeter's radiation is delayed also by the total count of free electrons (TEC) found in the layer above about 70 km [13]. Depending on solar cycle, solar illumination, etc, the TEC varies widely, causing an apparent increase in path length up to 25 cm. The optical path length delay due to TEC depends on frequency $f$ as $f$–2. Hence, simultaneous altimeter heights $h_1$ and $h_2$ obtained at two different

**Table 2. TOPEX Height Accuracy**

| Uncertainty Source | Height Error | Residual Uncertainty |
|---|---|---|
| Instrument $\delta h_A$ | | |
| Noise | ~25 cm | 2 cm |
| Waveform bias | ~25 cm | 3 cm |
| Timing bias | ~1 m | 1 cm |
| Surface interaction $\delta h_B$ | | |
| EM bias | ~0.05 × SWH | 2 cm |
| Skewness | ∝SWH | 1 cm |
| Propagation $\delta h_h$ | | |
| Ionosphere | 5 cm–25 cm | 1.3 cm |
| Dry troposphere | ~2.2 m | 0.7 cm |
| Wet troposphere | 5 cm–50 cm | 1.2 cm |
| Orbit $h_O$ | (large) | 3.5 cm |
| RSS error | >2.5 m | <5 cm |

frequencies $f_1 > f_2$ can be combined as

$$h = \frac{f_1^2}{f_1^2 - f_2^2} h_1 - \frac{f_2^2}{f_1^2 - f_2^2} h_2$$

to offset the unwanted ionospheric delay error. The TOPEX altimeter operates at Ku-band (13.6 GHz) and C-band (5.2 GHz), generating height estimates $h_K$ and $h_C$ respectively. The TOPEX algorithm that corrects for the ionospheric path length delay is $h = 1.18h_K - 0.18h_C$.

*Orbit determination* $h_0$ The dominant error in absolute height measurements from a radar altimeter is the uncertainty of the satellite's instantaneous radial distance from the reference ellipsoid. The perturbations on a satellite in low Earth orbit, in order of importance, include: variations in the gravity field; radiation pressures; atmospheric pressure; tides, both oceanic and solid Earth; and the troposphere. Real-time observation of the satellite's orbital perturbations is subject to errors also, compounded by insufficient knowledge of the Earth's geoid, and location uncertainties for the tracking systems.

The principal methods used by T/P for precision orbit determination (POD) rely on its global positioning (GPS) receivers and the Doppler Orbitography and Radiopositioning Integrated by Satellite data (DORIS) system. DORIS instantaneous navigation is better than 4 m on all axes, a tolerance which reduces to less than 5 cm (radial) after precision processing. T/P carries a set of optical retro-reflectors (corner cubes) mounted around the circumference of the altimeter antenna. When within view of ground stations equipped with precision range measurement lasers, the corner cubes can be illuminated. The resulting laser ranging measurements are used to calibrate the on-board orbit determination systems.

The radial orbit determination error for TOPEX/Poseidon has been reduced to less than 3.5 cm when averaged (RSS) over its orbital repeat period [14]. The predominant errors have 2 cm to 3 cm peaks, concentrated at a once-per-orbit frequency. Orbit determination residuals can be reduced through analysis of height measurements at locations at which the ascending and descending satellite orbits cross. After removal of all geophysical signals and adjustment for changes in the orbit, the measured heights at each cross-over point should be equal. Comparison of the actual cross-over differentials helps to refine the orbital models. For TOPEX, cross-over analysis of many orbits over a period of 30 to 60 days reduces the residual to about 2 cm. At this level of precision, inaccuracies in the Earth's tide and geoid models dominate the remaining error. Improvements in these models are expected to lead to 1 cm radial orbit accuracies for the Jason series of altimeters.

Such tight orbit determination is unlikely to be achieved in the near future for the radar altimeter satellites at 800 km altitudes. For example, the working objective for POD on GFO is 5 cm, based primarily on GPS tracking and dynamic modeling (although it was better than 7 cm only rarely between 1998–2002).

## THEORETICAL FOUNDATIONS

Altimeters generally fall into one of two kinds, determined by their beamwidth and range resolution. Radar altimeters illuminate the surface through an antenna pattern of width $\beta$, which typically is less than a few degrees. As a part of the on-board processing, the received energy is processed into resolved range shells. Beamwidth determines the width $\beta h$ of the surface illuminated by the antenna. As it intersects the surface, each range of resolved length $\rho$ also determines a surface area of width $2r_P$ [15]. Beam-limited radar altimeters are those for which $\beta h < 2r_P$. Conversely, $2r_P < \beta h$ for pulse-limited altimeters. The altimeters cited in Table 1 are all pulse-limited.

### Pulse-limited altimeters

Figure 3 illustrates the pulse-limited condition. The height accuracy of a pulse-limited altimeter is much less sensitive to (small) angular pointing errors than is the case for a beam-limited altimeter.

The pulse-limited radius $r_P$ of a quasi-flat surface on the Earth of mean radius $R_E$ is

$$r_P = \sqrt{c\tau h/\alpha_R} \tag{2}$$

where $\alpha_R = (R_E + h)/R_E$ is a consequence of the spherical observation geometry. For typical satellite radar altimeters, the pulse-limited footprint over a quasi-flat surface is on the order of two kilometers in diameter. The pulse-limited

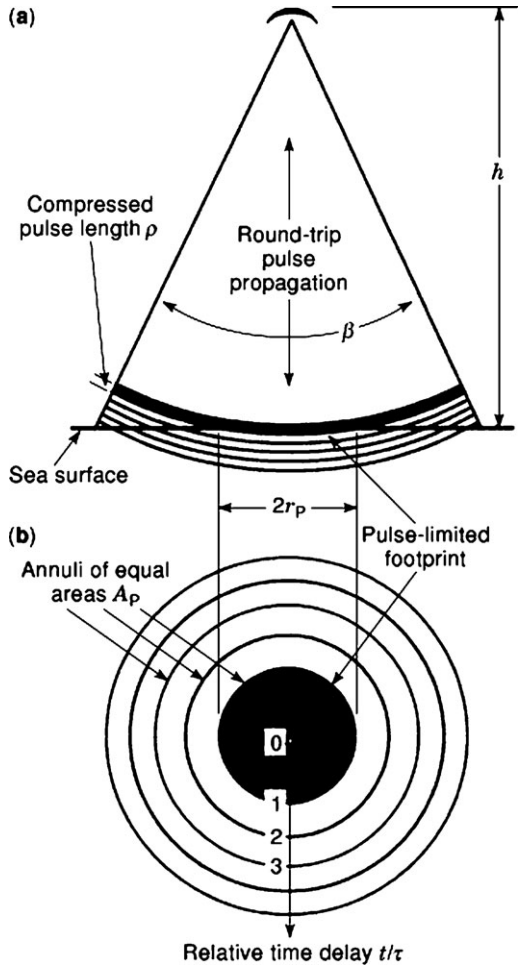


**Figure 3.** Elevation (a) and plan view (b) of a pulse-limited radar altimeter's illumination geometry. The surface area simultaneously illuminated within the duration of the compressed radar pulse length dominates the height measurement. This pulse-limited area expands for larger significant wave height (SWH).

area is

$$A_{\mathrm{P}} = \pi r_{\mathrm{P}}^2 = \frac{\pi c \tau h}{\alpha_R} \tag{3}$$

As the pulse continues to impinge and spread over the surface, the resulting pulse-limited annuli all have areas equal to that of the initial pulse-limited footprint. Hence, the received power tends to maintain the level corresponding to the peak of the initial response. The pulse-limited areas expand in response to increasing large-scale surface roughness, which in the oceanographic context is expressed as significant wave height SWH.

### Radiometric response

The classical single-pulse radar equation that describes the post-processing peak power $P$ is

$$P = \frac{P_{\mathrm{T}} G^2(\theta) \lambda^2 C_{\mathrm{R}} \sigma}{(4\pi)^3 h^4} \tag{4}$$

where $\sigma$ is the effective radar cross section, $P_{\mathrm{T}}$ is the transmitted power, $G(\theta)$ is the one-way power gain of the antenna as a function of off-boresight angle, $\lambda$ is radar wavelength, $h$ is height, and the range pulse processing gain (compression ratio) is $C_{\mathrm{R}}$. In the altimetry literature, the radar cross section usually is interpreted to mean $\sigma = \sigma^0 A_\sigma$ where $\sigma^0$ (sigma-0) is the normalized scattering coefficient (dimensionless) of the terrain, and $A_\sigma$ is the area of the resolved footprint. The peak power observed within a conventional radar altimeter, at the instant that the pulse-limited area at nadir is fully illuminated, is given from Eq. (3) and Eq. (4) by

$$P_{\mathrm{P}} = \frac{P_T G^2 \lambda^2 C_{\mathrm{R}} \pi c \tau \sigma^0}{(4\pi)^3 h^3 \alpha_R} \tag{5}$$

The power described by Eq. (7) is proportional to compressed pulse length $\tau$, and to the inverse cube of height $h^{-3}$.

### Flat surface response

Under reasonable conditions, the expected output $g(t)$ from any linear sensor is given by the convolution $g(t) = p(t)^* s(t)$ of the sensor's impulse response $p(t)$ over the distribution $s(t)$ that describes the input data source. A pulse-limited radar altimeter is an example of a linear system, but its response to input data takes on a special form due to the relatively strange geometry through which it views surface height variations. As a function of time, the radiating pulse first strikes the surface, and then spreads out over it. The so-called *flat surface response* is the altimetric counterpart to the generic impulse response function. It serves as the primary analytical basis for description of a radar altimeter's waveform from a variety of surface topographies.

In the altimetry literature two closely related "flat surface" functions appear, denoted here as $p_{\mathrm{I}}(t)$ and $p_{\mathrm{F}}(t)$. The (idealized) flat surface response $p_{\mathrm{I}}(t)$ was introduced originally [15] as a system function to account for the effects of antenna pattern, illumination geometry, and incoherent surface scattering. As an extension, Brown's [16] flat surface response $p_{\mathrm{F}}(t)$ includes the impact of the compressed pulse shape and signal processing as well as the functional dependencies captured in $p_{\mathrm{I}}(t)$. Brown's model is used most widely.

The difference between these two flat surface functions is subtle, but significant. The average input data distribution presented to a conventional radar altimeter is well-modeled by $s(t) = p_{\mathrm{I}}(t)^* q(t)$, which is a convolution of the (idealized) flat surface response $p_{\mathrm{I}}(t)$ with the topographic distribution $q(t)$ of the surface. The resulting radar altimeter linear model is the convolution $g_{\mathrm{A}}(t) = p_{\mathrm{F}}(t)^* q(t)$, where $p_{\mathrm{F}}(t) = p(t)^* p_{\mathrm{I}}(t)$ is Brown's flat surface response function, and $p(t)$ is the conventional linear system impulse response of the altimeter. The output $g_{\mathrm{A}}(t)$ is known as the altimeter waveform, examples of which are sketched in Fig. 2.

The flat surface response function (averaged) of a conventional satellite radar altimeter is

$$\begin{aligned} p_{\mathrm{F}}(t) = 0 \quad & \frac{1}{\tau}[t - \frac{2h}{c}] \le 0 \\ = \frac{t}{\tau} \quad & 0 < \frac{1}{\tau}[t - \frac{2h}{c}] \le 1 \\ = 1 \quad & 1 < \frac{1}{\tau}[t - \frac{2h}{c}] \end{aligned} \tag{6}$$

under the simplifying condition of a perfectly rectangular compressed unity pulse of length $\tau$. The defining characteristic of this response is that it is essentially a step function: following its linear rise over the duration of the compressed pulse, its maximum value is supported for many subsequent delay intervals. In practice, this waveform is attenuated in time due primarily to weighting of the antenna pattern away from boresight. Also, the waveform itself is more rounded, as a consequence of the weighted shape of the compressed pulse produced by a realistic altimeter.

## DERAMP ON RECEIVE

A satellite-based radar altimeter needs to measure the distance accurately, but only for an essentially planar surface, oriented orthogonally to the radar's line-of-sight. Conservative design suggests that all radar resources should be concentrated near the reflection from that surface. Hence, ocean-viewing altimeters have a small range window that tracks the delay and strength of the surface reflection. The ocean's surface has a significant wave height of less than 20 m or so, and its radar backscatter coefficient spans 3 dB to 20 dB, to cite parameters used in the testing of the TOPEX altimeter. In practice, range gate delay and backscatter tracking are met with two servo-regulator feedback loops (Fig. 4). The first loop is a second-order height tracker consisting of range position (alpha tracker) and range rate (beta tracker). The second loop is the receiver gain control (AGC). Altimeter height measurement is given by the setting of the range delay coarse and fine values, corrected by the remaining height error measured from the waveform's position in the tracker. Surface wind speed and significant wave height are derived from the AGC values and the waveform's shape, respectively.

The precision of an individual height measurement is determined by range resolution. If a simple short pulse were transmitted, then the height resolution would equal the pulse length. The principal disadvantage of a short pulse is that it contains little energy. The inherent resolution of a pulse is inversely proportional to its bandwidth. Most radar altimeters use some form of modulation on the transmitted signal to maintain a large bandwidth within a longer pulse, thus increasing the transmitted energy at no loss of resolution. A well-established modulation technique used in many airborne radar altimeters is frequency-modulated continuous wave (FM-CW), from which height is proportional to the frequency difference between the transmitted and received signals. An alternative approach is pulse compression, whereby a relatively long large time-bandwidth pulse is transmitted, and then processed (compressed) after reception to a simple short pulse of unity time-bandwidth.

Satellite-based radar altimeters use a different and specialized form of modulation and demodulation. The relatively distant and narrow range window typical of an ocean-viewing satellite radar altimeter is ideal for the full deramp (stretch) technique [17] which was first applied to altimetry by MacArthur [18] in the Seasat altimeter. The defining feature of the full-deramp technique is that the transmitted pulse length is longer that the depth of the range window.

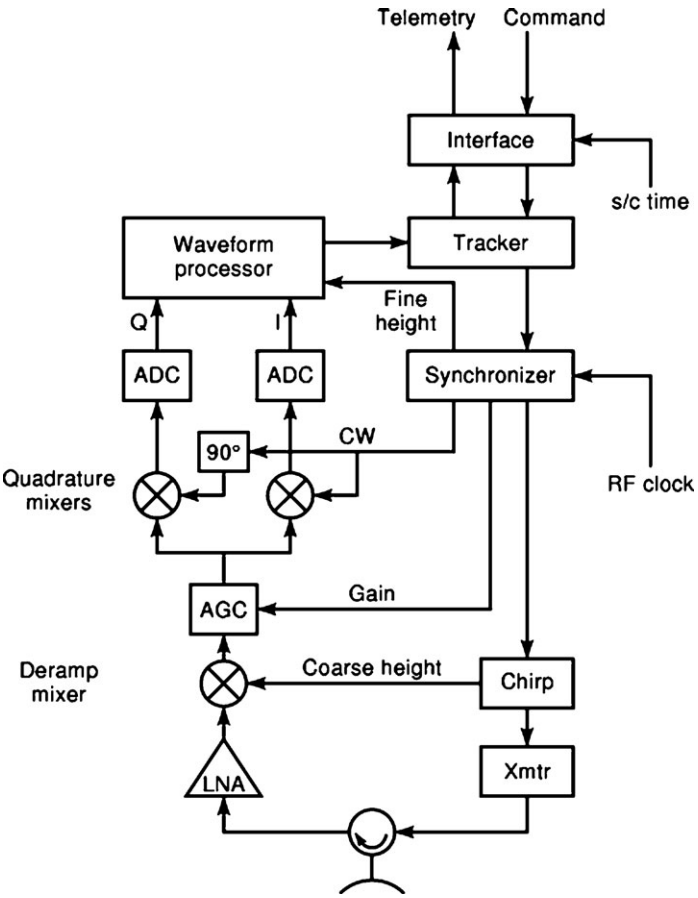


**Figure 4.** The functional diagram of a modern satellite altimeter is centered on the waveform tracker, whose outputs are: (1) translated into science data to be returned *via* telemetry, and (2) transformed into closed loop timing and gain controls for the radar.

The full deramp (dechirp) technique employs a transmitted chirp (linear FM signal) of duration $T_P$, bandwidth $B_P$, chirp rate $k_P$, and center frequency $f_0$. For a pulse initiated at $t = 0$, the transmitted frequency is $f_0 + k_P\, t$, $t \in T_P$, as shown in Fig. 5. The bandwidth is $B_P = k_P\, T_P$, and the associated time-bandwidth product is $k_P\, T_P^2$. Pulse bandwidths and the time-bandwidth products for satellite radar altimeters are large, on the order of 300 MHz and 30,000 respectively. The compressed pulse length $\tau$ is given by the inverse bandwidth of the transmitted pulse, or alternatively, by the original pulse length $T_P$ divided by the time-bandwidth product. Thus, a full deramped altimeter's height resolution is

$$\tau = \frac{1}{k_P T_P} \text{ seconds} \quad \text{or} \quad \rho = \frac{c}{2\, k_P T_P} \text{ meters} \tag{7}$$

The altimeter tracking system anticipates the time $t_0$ when the reflected signals will arrive back at the radar. To meet these, another chirp is generated, at time $t_c \approx t_0$ and center frequency $f_0 - f_I$, where $f_I$ is to become the receiver's intermediate frequency (IF). (The deramp chirp time $t_C$ in general is slightly different from $t_0$, as explained in the tracking discussion below.) The deramp chirp is mixed with the incoming signals, after which their difference frequen-

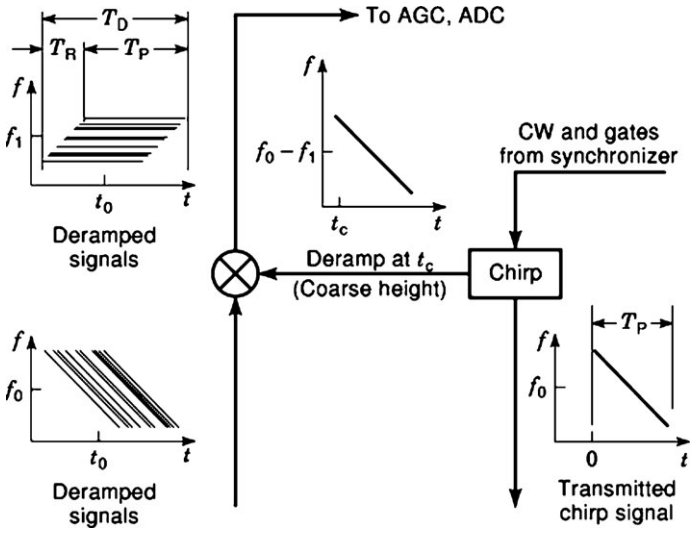


**Figure 5.** A long linearly frequency-modulated (chirp) pulse is transmitted (as in Fig. 4), followed by full deramp demodulation on receive to produce a relatively narrow band set of CW data signals at intermediate frequency $f_1$.

cies are retained, to produce the set of deramped data signals shown in the figure.

The key to many characteristics unique to a radar altimeter lies in this deramp domain. The deramped signal from the $m^{\text{th}}$ individual scatterer at time delay $t_{\text{m}}$ is a CW segment of length $T_{\text{P}}$ and frequency

$$f_m = 2k_p(t_m - t_C), \quad t_m \in T_R \tag{8}$$

where $T_{\text{R}}$ is the time spanned by the received signals. For a range window $R_{\text{H}}$ meters deep, $T_{\text{R}} = 2R_H/\text{c}$. The IF bandwidth $B_{\text{I}}$ is determined by the FM rate and the range window, $B_{\text{I}} = 2\,k_{\text{P}}\,R_{\text{H}}/\text{c}$. If the range depth of the scene is small, as is the case with radar altimeters meant to operate over the ocean, then the corresponding IF bandwidth is small, typically less than 5 MHz. Clearly, the full deramp technique offers a considerable savings in system bandwidth at all subsequent stages, and at no cost in range resolution.

The deramped window duration $T_{\text{D}} \geq T_{\text{P}} + T_{\text{R}}$ must be larger than the pulse duration to accommodate the extra time induced by the range window time span. The full deramp technique works best when $T_{\text{P}} > T_{\text{R}}$, a condition that is very well satisfied for oceanographic altimeters for which $T_{\text{R}}$ is less than 1% of $T_{\text{P}}$.

Alert: there is a conceptual pitfall lurking in the deramped signal domain. Time and frequency reverse their customary roles. In this domain, time delay is no longer a measure of the radar range to reflectors. Rather, the signals' time duration $T_{\text{P}}$ determines their compressed pulse resolution according to Eq. (7), and thus "time" behaves as a bandwidth. Conversely, each scatterer's round-trip time delay, relative to the track point, is proportional after deramp to the CW frequency given by Eq. (8), relative to the IF center frequency. Thus "frequency" behaves as delay time, which is proportional to radar range.

## THE TOPEX DESIGN

The TOPEX Ku-band altimeter [10,11,18] illustrates the essential features of conventional space-based radar altimeters (Fig. 4). The TOPEX altimeter is controlled by a synchronizer whose inputs are derived from the tracker outputs, slaved to a master radio frequency clock at 80 MHz. The tracker and synchronizer control the altimeter in all seven of its operational modes: test, calibrate, stand-by, coarse track acquisition, fine track acquisition, coarse resolution track, and fine resolution track. Table 3 lists values for selected TOPEX parameters.

In the fine resolution track mode, the radar transmits a linear-FM (chirp) pulse of length 102.4 $\mu$s and bandwidth 320 MHz. The signal generator consists of a digital section that creates 40 MHz chirps at baseband, followed by RF sections that multiply and mix the signals to meet the final bandwidth and center frequency. The chirped pulses at 13.6 GHz are amplified in a traveling wave tube to 20 W (peak), and transmitted at 4.5 kHz pulse repetition frequency (PRF) through an antenna 1.5 m in diameter.

The received pulses are amplified and then mixed with a delayed chirp signal, centered at 13.1 GHz to produce an ensemble of CW data signals spread over a band of $\sim$3 MHz about an intermediate frequency of 500 MHz. The deramped data signals are further amplified, subject to gain control in the AGC attenuator, mixed down to in-phase and quadrature video, low-pass filtered and digitized. At this stage, the low-pass filter has the effect of removing echoes from ranges that are well outside of the desired range gate window. The signals are magnitude-squared, and summed to produce smoothed height waveforms. Extensive waveform averaging over statistically independent samples is essential to suppress the speckle noise that otherwise would dominate the waveforms. The smoothed waveforms are processed to extract the data of interest, and the tracking outputs are fed back to close the control loops of the radar.

The Ku-band and the C-band channels are time-multiplexed, which impacts system timing from the PRF to the processor.

### Sampling and Waveform Processing

The mean amplitude of the deramped signals is normalized through an automatic gain control (AGC) amplifier. The receiver gain is set by the level observed in the waveform processor. Signal level is proportional to the scattering coefficient (sigma-0) of the water's surface, which in turn is a function of surface wind speed. The normalized signals in the TOPEX altimeters are mixed down to in-phase (I) and quadrature (Q) video channels and passed through 625 kHz low-pass filters prior to analog-to-digital sampling at a 1.25 MHz rate. This produces a set of 128 complex samples uniformly spaced over the 103.2 $\mu$s deramp interval $T_{\text{D}}$.

The tracker and synchronizer control the position of the altimeter height settings through two paths: coarse, and fine. The coarse height feedback depends on the deramp trigger $t_{\text{C}}$ that is slaved to the 80 MHz clock, which has a period of 12.5 ns. Thus, choice of $t_{\text{C}}$ is restricted to a set

**Table 3. TOPEX Chirp Parameter Values**

| Parameter | Symbol | Value | Units |
|---|---|---|---|
| Chirp rate | $k_P$ | −3.125 | MHz/μs |
| Pulse duration | $T_P$ | 102.4 | μs |
| Pulse bandwidth | $B_P$ | 320 | Hz |
| Time × bandwidth | | 32,768 | (nil) |
| Pulse resolution | $\rho$ | 0.469 | m |
| Pulse resolution | $\tau$ | 3.125 | ns |
| Carrier ($K_u$-band) | $f_0$ | 13.6 | GHz |
| Carrier (C-band) | $f_0$ | 5.2 | GHz |
| IF frequency | $f_1$ | 500 | MHz |
| IF bandwidth | $B_1$ | 3 | MHz |
| Range time span | $T_R$ | 400 | ns |
| Deramp time span | $T_D$ | ~103 | μs |

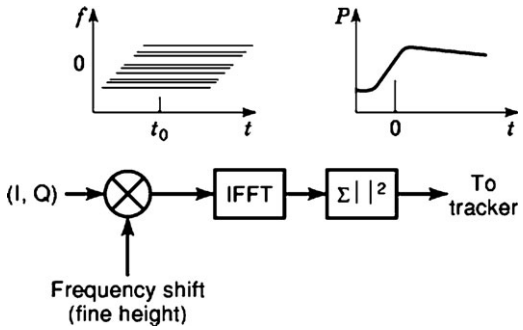


**Figure 6.** The waveform processor (see Fig. 4) of a pulse-limited radar altimeter performs three basic functions: (1) application of a frequency shift to effect the fine range-delay correction, (2) an inverse FFT applied to each return to transform the CW signals into a power distribution as a function of altimetric height (relative to the track point), and (3) summation over many of these individual power waveforms to form the averaged waveform which is sent to the tracker.

of discrete delays separated by 12.5 ns, corresponding to height intervals of 1.875 meters each. The fine height feedback is exercised in the digitized deramp domain (Fig. 6). In the deramp domain, a small frequency shift is equivalent to a small time delay $\Delta t$. For a fine time shift interval $-12.5 \text{ ns} < \Delta t < 12.5 \text{ ns}$, the corresponding frequency shift is $k_P \Delta t$, bounded by $\pm$ 39.0625 kHz. The 25 ns fine time shift adjustment interval is large enough to accommodate anticipated range rates without having to reset the course height feedback selection within one waveform processing cycle.

Following frequency shift, the data are inverse Fourier transformed (IFFT) and magnitude-squared detected. The IFFT converts CW to time shift (relative to the track point), and compresses the data to its individual pulse resolution, 0.469 meters. Each resulting waveform is a distribution of power across the bins within the range window (as suggested in Fig. 2).

As is true for most radars, the received waveform produced by an individual pulse is corrupted by speckle noise. Speckle is created by the coherent interference within a given echo between unresolved and competing elementary scatterers, and causes the signal's standard deviation to be large. (In the limit, the standard deviation equals the signal's mean value for an individual waveform drawn from a Gaussian ensemble). The standard deviation of the speckle can be reduced by summing (averaging) many statistically independent waveforms together. Statistical independence between sequential returns observed by a radar altimeter depends primarily on the radar pulse repetition rate (PRF), the antenna size, the spacecraft velocity, and on the sea surface conditions [19]. The pulse-to-pulse statistical independence threshold for TOPEX is about 2.5 kHz, yet its PRF = 4.5 kHz. The pulse rate above the threshold improves the additive SNR, but does not contribute to speckle reduction.

## Tracking

The TOPEX Ku-band channel averages 228 pulses over a so-called track interval of about 50 ms to produce the smoothed waveforms delivered to the tracker at a 20 Hz rate. For each waveform, the range window (Fig. 2) is partitioned into 128 sample positions or bins, each of size equal to the radar's range resolution. Groups of bins are organized into *tracking gates* of various sizes whose outputs are used to calculate the parameters that control the altimeter's feedback loops, and to provide the first-order science data from the instrument [20]. The tracking algorithm, based on an Intel 80186 microprocessor, iterates at the waveform input rate of 20 Hz. Each tracking gate is normalized so that its gain is inversely proportional to its width, which is the number of samples that it spans. The range width of each gate is a power of two times the intrinsic range resolution of the altimeter.

The noise gate estimates the mean noise level from samples 5 through 8, which occur well before the waveform begins to respond to surface reflections. The mid-point of the waveform's leading edge is tracked to keep it centered between samples 32 and 33. The AGC gate spans samples 17 through 48, which are centered on bin 32.5, the so-called *track point*.

The output of the AGC gate is fed back to control the altimeter's gain loop. TOPEX is required to measure waveform power (proportional to sigma-0) with an accuracy of $\pm$ 1 dB and a precision of $\pm$ 0.25 dB. In response to the waveform levels observed in the AGC gate, the receiver attenuator is adjusted in 1 dB steps. To meet the accuracy and precision requirements, from pulse to pulse the attenuator setting is dithered between neighboring steps. This has the effect of interpolating the mean AGC setting to an effective accuracy of less than 0.1 dB when averaged

over all 228 input waveforms. Waveform power (sigma-0) returned as science data is equal to the mean AGC level plus the AGC tracking gate level.

To summarize, the altimeter's measurements are: SSH – the position of the track point, plus the track-point offset; SWH – proportional to the width of the waveform leading edge of the waveform; and WS – proportional to a function (empirically determined) of 1/(waveform power), hence derived from the AGC setting.

## GRAVITY AND BATHYMETRY-PRECISION

Radar altimetric data are the basis for state-of-the-art geodesy expressed through the ocean's surface, and consequently, global bathymetry. The principal objective of a geodetic satellite radar altimeter [21] is to measure the (along-track) slope of the sea surface caused by gravity deflections over spatial scales less than a few hundreds of kilometers (Fig. 7). Sea surface slope is derived by taking the difference between two neighboring height measurements, where the slope tangent equals "rise over run". The key word for these measurements *is precision*: the standard deviation (noise) of the sea surface height measurement about its mean value. Height measurement precision is determined by the radar altimeter's post-processing range resolution, and by the amount of averaging available for each estimate. Note that a precision measurement may still have poor accuracy, if its mean value is biased away from the correct value. When comparing two neighboring height measurements, any constant bias is cancelled by differentiation as long as the error is the same for both measurements. The sea surface slope measurement problem is challenging because the desired slope signals are as small as 6 mm height differential (rise) for each 6 km along-track separation (run). Such a slope corresponds to one microradian of gravity deflection, or about a one milligal gravity anomaly.

In addition to height precision, geodetic altimetry requires smaller along-track resolution than a conventional altimeter, and a suitable orbit. The altimeter's footprint resolution should be smaller than about 6 km, which corresponds to the minimum half-wavelength scale of the observable gravity anomaly spectrum. The orbit should not repeat for ~1.2 years, to yield an average ground track spacing of 6 km, again in respect of the anomaly spectrum. The orbit's inclination should be near 50°–63° (or 113°–120° retrograde) to resolve north and east slopes nearly equally, and to cover the lower latitudes where existing data are inadequate. Note that oceanographic radar altimeter missions (TOPEX/Poseidon, Jason-1, ERS1/2, Envisat, and Geosat ERM/GFO) normally are placed into exact-repeat orbits (10 to 35 days), and as a consequence have widely spaced (80 km to 315 km) ground tracks. Such orbits cannot resolve the short-wavelength two-dimensional surface slopes required for useful bathymetry.

Since absolute height accuracy is not required, geodetic radar altimeters can be relatively basic instruments. They do not need to compensate for propagation delays, hence they need only one frequency, and they do not need a water vapor radiometer. Indeed, such an instrument is

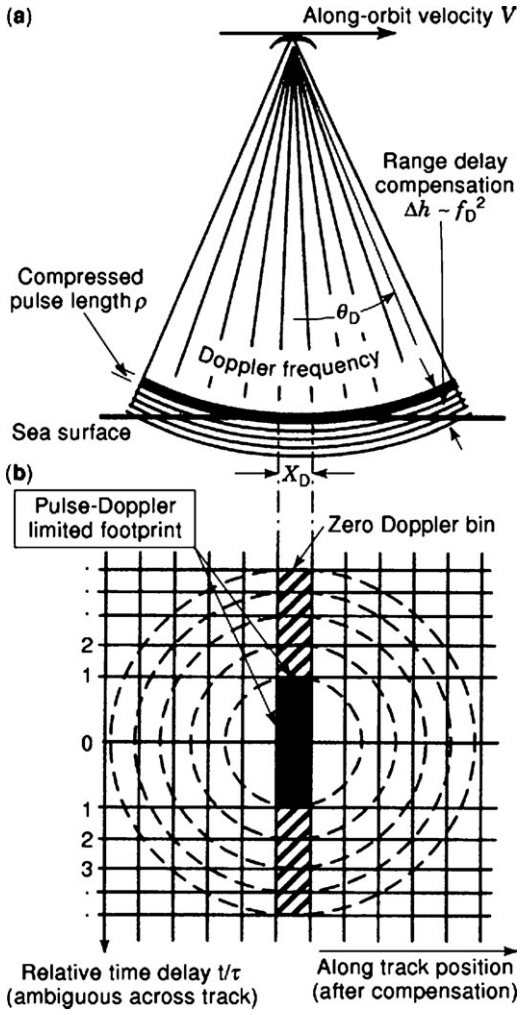


**Figure 7.** The ocean's bottom topography causes subtle variations in the local gravity field, which are expressed as small tilts in the ocean's surface. These are observable by satellite altimetry.

preferred; it has been shown that efforts to correct for path delays usually add noise to slope estimates [22]. Geodetic measurements provided by the Geosat and ERS-1 (both single-frequency altimeters with no WVR) furnish the best resolution oceanic gravity from space to date. Their resulting bathymetric resolution is limited to about 25 km north-south, and poorer resolution of east-west slope components. These results reflect the less-than-optimum resolution, waveform precision, and orbit inclination of those two altimeters. Geodetic resolution at the ocean's surface can be no finer than about 6 km (half wavelength), a limit that is determined by the average depth of the ocean.

Gravity anomalies are caused by topographic relief on an interface between two volumes of differing mass density. In the deep ocean, sediments are thin, and the basaltic sea floor crust is internally flat-layered, and so gravity anomalies at the surface reflect the topography of the ocean floor. Conversely, at continental margins the sea floor is nearly flat and sediments are generally thick. Beneath these sediments there may be basins or other geologic structures of interest. In such regions, surface slope signals are due pri-

marily to topographic variations at the interface between crystalline rocks and their sedimentary overburden. The sediment/basement interface provides essential reconnaissance information for petroleum exploration. The correlation between slope and existing depth soundings readily distinguishes these two environments [23].

The slope signals required to estimate bathymetry are band-limited (12 km to 300 km full-wavelength), as determined by fundamental physical principles. Hence, the height measurements of a geodetic altimeter need to maintain relative accuracy–precision–only over this relatively narrow band.

Within this band, precision turns out to be the dominant limiting condition. Sea surface slope measurements are derivatives of the altimeter's natural measurements, height. Taking derivatives eliminates constant and long-wave height errors, but it amplifies noise at short wavelengths. Using a simple model in which height errors are assumed to be a Gaussian white noise process over the geodetic band, the one-sigma slope error is about 1.8 $\sim$rad if the altimeter's one-sigma height precision is 1 cm for a one-second averaged height value. Experience teaches that height precision degrades with increasing significant wave height (SWH). One of the factors that motivated the development of the delay-Doppler approach to radar altimetry was to improve measurement precision.

## DELAY-DOPPLER

The delay-Doppler technique leads to better measurement precision, a smaller effective footprint at nadir, and increased tolerance of along-track surface gradients typical of continental ice sheets. The central innovation in the delay-Doppler concept [24, 25] is that it combines the benefits of coherent and incoherent signal processing, rather than relying exclusively on incoherent averaging as is the case for all conventional satellite radar altimeters. The coherent processing stages, patterned after well-established methods developed for synthetic aperture imaging radar (SAR), allow much more of the instrument's radiated power to be converted into height measurement data. One consequence of delay-Doppler signal processing is that less transmitted power is required than with a conventional altimeter. The delay-Doppler technique also enjoys the benefits of the pulse-limited range measurement geometry.

The coherent processing transforms groups of data into the Doppler frequency domain, where delay corrections are applied, analogous to SAR range curvature correction [26]. Doppler processing determines the size and location of the along-track footprint, which is (1) smaller than the pulse-limited diameter, (2) a constant of the system, and (3) relatively immune to surface topographic variations. Waveforms are incoherently summed corresponding to each surface position as the altimeter progresses along track. One direct result is that each height measurement from a delay-Doppler altimeter has more incoherent averaging than is possible from a conventional radar altimeter.

The delay-Doppler technique exploits coherence between pulses, in contrast to the pulse-to-pulse incoherence that is the norm for conventional pulse-limited altimeters. Pulse-to-pulse coherence requires that the PRF be above the inter-pulse correlation threshold, rather than below it as is normal for conventional incoherent radar altimeters [19]. To assure correlation, the PRF must be high enough so that at least two pulses are emitted while the satellite's forward motion equals the along-track aperture size of the altimeter's antenna.

### Delay-Doppler domain

The objective of delay compensation is to remove the extra delay (Fig. 8) that is induced by the spherical curvature of the radar's ranging wavefront as it impinges on the ocean's surface. At each along-track angular offset $\theta_D$ from nadir, there is an extra range distance $\Delta h = h(\sec\theta_D - 1)$ due to range curvature. As it is received, the signal includes returns from scatterers at many different angles. Hence, the problem is multi-valued; in the signal domain compensation for wavefront curvature is impossible. This is the situation for conventional incoherent radar altimeters. In the delay-Doppler altimeter, however, along-track coherent processing gets around this dilemma. Transformation from the signal domain to the frequency (Doppler) domain reduces delay compensation to a single-valued problem: at each Doppler frequency $f_D$ the extra range-delay increment is unique, and known.

The delay increment, in terms of Doppler frequency $f_D$ as its independent variable, is

$$\Delta h(\ f_D) \approx \alpha_R \frac{\lambda^2 h}{8V^2}\ f_D^2 \tag{11}$$

where $V$ is the velocity of the spacecraft along its orbit. Recall that the deramped data in the range direction appear as constant (CW) frequencies. Each range delay increment translates into an equivalent CW frequency shift. These unwanted frequency shifts may be nullified by multiplying the data field by equal and opposite CW signals prior to the range IFFT, analogous to the fine tracking frequency shift of a conventional radar altimeter. The result is evident in Fig. 9, which compares the flat surface response waveform (as it would appear in the delay-Doppler domain) before and after delay compensation.

### Implementation

The delay-Doppler altimeter introduces additional along-track processing steps (Fig. 10) after the range deramp and before the range IFFT. The net effect of the extra processing is to transform the signal space from one to two dimensions. A Fourier transform is applied to these data in the along-track dimension, implemented in real time on-board as a set of parallel FFTs that span the range window width. Signals in the resulting two-dimensional deramp/Doppler domain are phase shifted to eliminate the unwanted range.

The delay correction phase functions are

$$\Phi(\ f_D, t) = \exp\{+\,j2\pi k_P \frac{2}{c}\,\Delta h(\ f_D)t\} \tag{12}$$

which are CW signals whose frequency is matched to the delay increment given by Eq. (11). The data at this stage consist of an ensemble of two-dimensional CW signals. Fre-

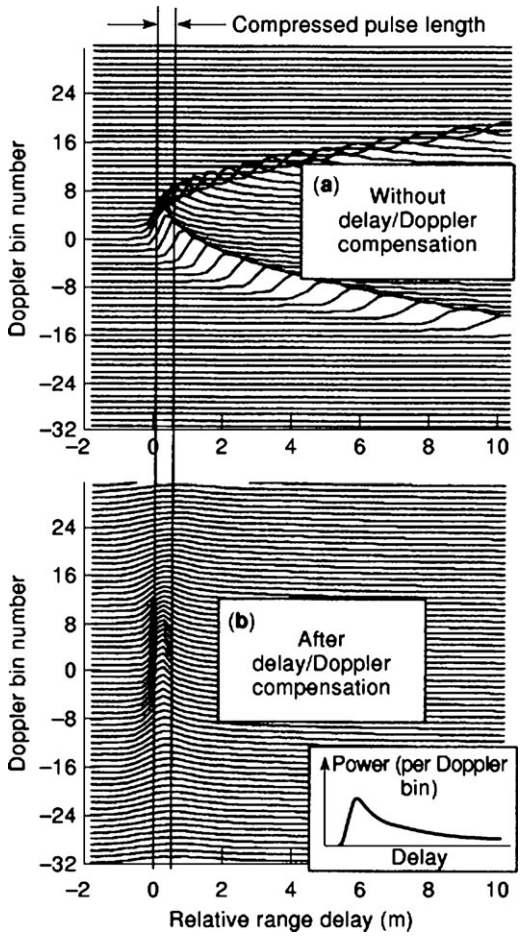


**Figure 8.** Elevation (a) and post-compensation plan view (b) of a delay/Doppler radar altimeter's illumination geometry. The resolved along-track footprint $X_D$ is Doppler-limited. The cross-track footprint is pulse-limited. Although the footprint is smaller than the pulse-limited area, more averaging is available at each Doppler bin position.

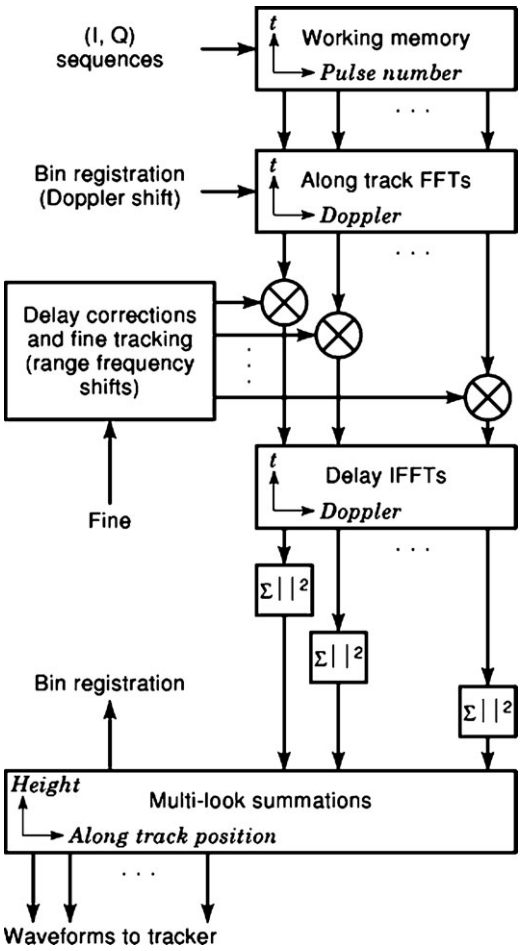


**Figure 9.** Simulated height waveforms, as they would appear in a compressed pulse (delay) and Doppler data array before (a) and after (b) curvature compensation, illustrate how delay/Doppler processing shifts more of the reflected energy into the pulse-limited region, thus improving the height estimates.

quency in the time delay direction is proportional to (minimum) delay relative to the range track point, and frequency in the along-track direction is proportional to the scatterer's along-track position relative to the zero-Doppler position.

The remaining data processing is carried out in parallel, consisting of a range IFFT at each Doppler frequency bin, detection, and assignment of the height estimates to their respective along-track positions. The process is repeated over subsequent blocks of data, from which many looks are accumulated at each along-track position. As the altimeter passes over each scatterer, the corresponding height estimates move in sequence from the highest Doppler filter to each lower frequency filter, until the scatterer is out of sight. Thus, the final waveform at each along-track position is the average (incoherent sum, normalized) of estimates from all Doppler filters. If the Doppler filters are designed to span the along-track antenna beamwidth, then all data along-track contribute to the height estimates. The resulting coverage is shown in Fig. 11, which contrasts the "scanning" beam of a conventional altimeter with the "mini-spotlight staring" Doppler-processed beam of a delay-Doppler altimeter. The figure shows the unfolding coverage of one resolved along-track cell; all illuminated cells are tracked in parallel through the Doppler filters, in similar fashion.

### Footprint

Delay-Doppler processing may be interpreted as an operation that flattens the radiating field in the along-track direction. In this transformed data space (Fig. 8(b)), the $(x,y)$ cells have constant along-track length, but their cross-track widths decrease as the square root of delay time. The cross-track footprint is determined by the pulse-limited condition.

The along-track impulse response is set up by the Doppler filters. Along-track impulse position is determined by the zero-Doppler position for each burst of data. Along-track position can be adjusted by artificial Doppler shifts to maintain registration of subsequent Doppler bins, which is the along-track analog of the fine height adjustment in an incoherent radar altimeter.

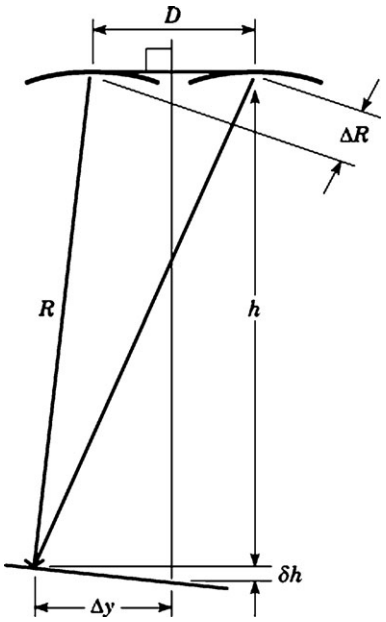


**Figure 10.** A delay/Doppler radar altimeter waveform processor (see Fig. 4) must be augmented with a cache memory to store the deramped returns from a sequence of transmitted pulses. FFTs are applied across these data to derive their Doppler frequency spectra, which then are corrected for curvature delay by phase multiplication.

Ideally, the along-track zero-Doppler position is equivalent to the geometric sub-satellite point, nadir. The along-track location of the zero-Doppler plane is independent of satellite attitude, and also is independent of terrain slope. Thus, the height measurements at all Doppler frequencies can be located along-track with respect to zero Doppler. In practice, the zero Doppler bin location may not coincide with nadir. A vertical spacecraft velocity component adds a Doppler shift to the signals. Vertical velocity and its implied Doppler error can be estimated. Offsetting Doppler shifts can be applied in response to a spacecraft vertical velocity component to assure registration of the Doppler bins with their corresponding along-track positions defined with respect to nadir.

### Unfocused condition

The foregoing is predicated on a simple isometry between Doppler frequency and along-track spatial position. This equivalence is valid for an along-track resolution that is comparable to or larger than the first Fresnel zone. In synthetic aperture radar parlance, this zone is known as the unfocused SAR resolution. Using the classic quarter wavelength criterion, the radius $a_0$ of the first Fresnel zone is

$$a_0 = \sqrt{\frac{h\lambda}{2}}$$

which for a Ku-band altimeter leads to an along-track (unfocused) dimension of 180 m from an altitude of 800 km (or about 230 m from an altitude of 1334 km). As these quantities are less than the nominal delay-Doppler along-track cell size of 250 m, the processing task is trivial: no focusing

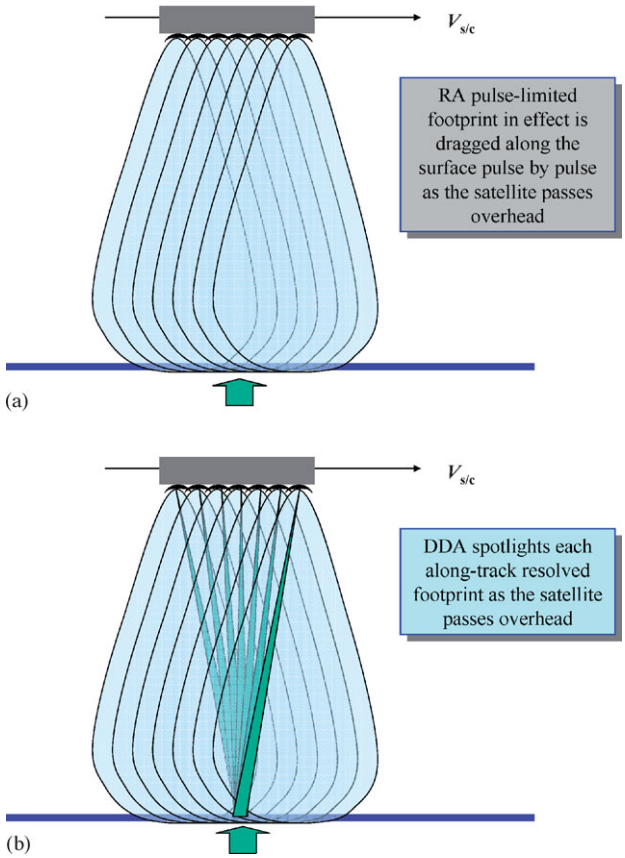


**Figure 11.** The delay-Doppler altimeter tracks cells resolved along-track (b) through the on-board processor, in contrast to a conventional altimeter (b) that in effect drags its footprint along the surface.

is required. Focus operations would be required if the Fresnel radius were larger than the along-track cell dimension. If a smaller cell size is desired such as for altimetry over land, or a very high satellite altitude or longer radar wavelength were chosen, then the along-track processor would have to incorporate phase matching to focus the data.

### Incoherent Averaging

There are two stages in a delay-Doppler altimeter at which incoherent averaging takes place: within each Doppler bin, and across neighboring bins. Detected returns from many pulses are averaged together to build the multi-look waveform within each bin. For a typical satellite altimeter, these waveforms would accumulate wihin each 250-m bin at about a 26 Hz rate. Subsequent averaging (incoherent integration) over adjacent waveforms typically extends over 0.1 s (or 1.0 s), during which time the antenna illumination pattern progresses in the along-track direction by an appreciable distance, approximately 0.6 km (or 6 km). Alert: the relative location of each delay-Doppler-derived height estimate is synchronized to coincide with the forward motion of the instrument, thus eliminating along-track elongation of the footprint as is the case for a conventional al-

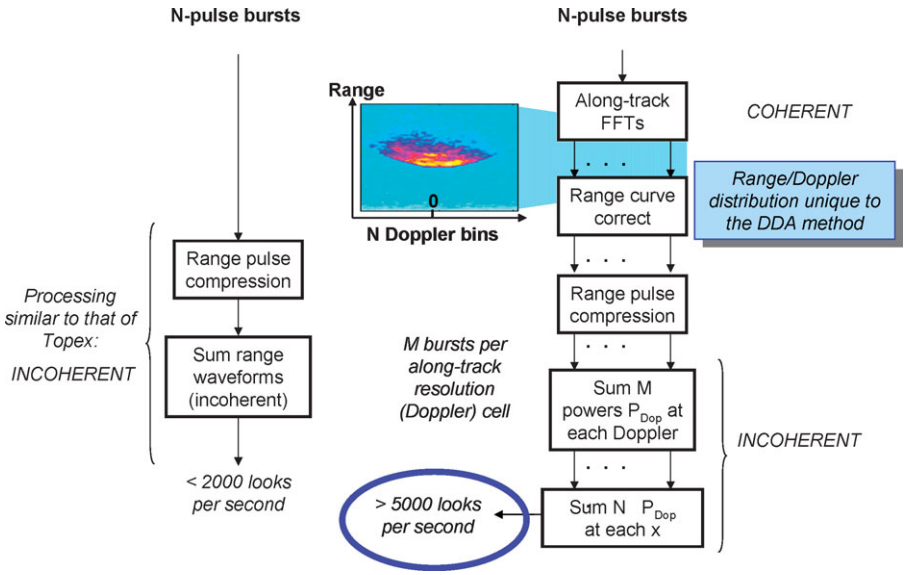


**Figure 12.** DDA processing increases the number of independent samples of the surface return, which reduces the intrinsic noise, thus improving the sea surface height measurement precision.

timeter. The result is that a delay-Doppler altimeter generates significantly more incoherent averaging than a conventional altimeter, and at less compromise in along-track footprint size (Fig 12).

One immediate benfit is better measurement precision. Consider the case of height precision in the context of geodetic requirements. Figure 13 shows a plot of height precision *versus* SWH for a delay-Doppler altimeter and a conventional radar altimeter (RA). The plot shows that the DDA meets the height precision requirement of 1 cm at 3 m SWH, a result that is consistent with previous analyses [27]. The figure also shows that the DDA is about half as sensitive as an RA to increasing SWH. This is important for geodetic applications, as measurement precision degraded by larger significant wave heights is a major source of noise in Geosat surface slope estimates [6].

## Flat surface response

The customary concept of flat surface response applies only to the delay time dimension for a delay-Doppler altimeter. This means that the inherent delay/elevation ambiguity characteristic of pulse-limited altimeters is reduced from two spatial dimensions to only one dimension. The cross-track ambiguity that remains is suggested in Fig. 8, which shows that at any given Doppler frequency, there are two possible sources for reflections having a given (relative) time delay. These arise from either side of the minimum delay locus, which nominally is the sub-satellite track. Of course, the point of first reflection (at zero relative delay time) may be to one side of the sub-satellite track, as would be true in general when there is a non-zero cross-track terrain slope. The cross-track ambiguity and the delay/elevation ambiguity both may be at least partially resolved through application of other means such as the monopulse phase sensing technique.

The flat surface delay time response (after processing) of the delay-Doppler altimeter has the functional form

$$\begin{aligned} f_{\mathrm{D}}(t) &= 0 && \frac{1}{\tau}[t-\frac{2h}{c}] \le 0 \\ &= \sqrt{\frac{t}{\tau}} && 0 < \frac{1}{\tau}[t-\frac{2h}{c}] \le 1 \\ &= \sqrt{\frac{t}{\tau}} - \sqrt{\frac{t}{\tau}-1} && 1 < \frac{1}{\tau}[t-\frac{2h}{c}] \end{aligned} \qquad (13)$$

where $\tau$ is the compressed pulse length (Eq. 7). The curve of Eq. 13represents the (average) strength of the altimeter's response to illumination of a quasi-flat surface as a function of time delay, just as in the conventional case. Note that the response to a flat surface for all regions $t < \tau$ have much less relative power for the delay-Doppler altimeter than for the conventional radar altimeter described by Eq. (6). The cross-track (time-delay) width of $f_{\mathrm{D}}(t)$ is approximately equal to $\tau$.

## Radiometric response

The delay-Doppler altimeter can take advantage of reflections from the entire length of the antenna illumination pattern in the along-track direction to estimate the height of each resolved patch of sub-satellite terrain. This implies that substantially more integration is possible than in a pulse-limited altimeter. Under the assumption that the dominant scattering mechanism is non-specular, the integration gain is linear in power. It follows that the total power arising from each resolved cell is larger for the delay-Doppler altimeter than for a conventional pulse-limited altimeter, even though the post-processing footprint size is smaller.

Height estimation for each resolved scattering cell benefits from integration as long as that cell is illuminated by the antenna pattern. For each scattering cell, the equivalent along-orbit integration is governed by the length $\beta h$ of the antenna footprint, expanded by the orbital factor $\alpha_{\mathrm{R}}$. The along-orbit integration may be interpreted in terms of

an equivalent along-track area $A_D$ that contributes to the received signal power for a delay-Doppler altimeter on a single-pulse basis. The cross-track dimension is set by the pulse-limited condition. Thus,

$$A_D = 2h\beta\sqrt{c\tau\alpha_R} \tag{14}$$

The post-processing power of the delay-Doppler flat-surface response function is

$$P_D = \frac{P_T G^2(\theta)\lambda^2 C_R \sigma^0}{(4\pi)^3 h^{5/2}} 2\beta\sqrt{c\tau\alpha_R} \tag{15}$$

which has an $h^{-5/2}$ height dependence, and a square-root dependence on compressed pulse length. The height dependence in Eq. (15) is the geometric mean between $(h^{-3})$ for the pulse-limited case described by Eq. (5) and $(h^{-2})$ for the beam limited case. Reduced sensitivity to compressed pulse length $\tau$ in comparison to the pulse-limited case may be helpful in system optimization.

From Eqs. (4) and (15), the relative power efficiency of the two altimeters is given by the ratio

$$\frac{P_D}{P_P} = \alpha_R \frac{A_D}{A_P}$$

in which it is assumed that all other factors (such as average transmitted power and antenna gain) are equal in the two cases. The areas $A_D$ and $A_P$ are given by Eqs. (3) and (14) respectively. To first order, the relative radiometric advantage of the delay-Doppler altimeter over the pulse-limited altimeter is given simply by the ratio of the equivalent areas over which the signals are integrated. Example: The delay-Doppler technique would require only about 1/10 of the transmitter power of TOPEX to support the same SNR performance, yet it yields waveforms with reduced speckle due to increased incoherent summation.

### Cross-track interferometry

Pulse-limited radar altimeters work best over relatively mild topographic relief of mean slope zero, such as the ocean's surface. Over ice sheets or terrestrial surfaces, performance is degraded. Unwanted characteristics include footprint dilation over rougher terrain, height errors in proportion to surface mean slope, and the tendency of the footprint location to hop from one elevated region to another (without the control or knowledge of the data analyst). Beam-limited techniques, of which laser altimeters are extreme examples, circumvent these problems, but may imply their own set of disadvantages.

A major potential application of radar altimetry is to monitor the height of extensive ice sheets, as found in Greenland or Antarctica. Approximately 95% of these surfaces have slopes less than ~3 degrees, which is sufficient to trick a conventional altimeter into very large height errors. For example, an unknown one-degree slope would lead to a 120-m surface height error, which is unacceptable. Although the delay-Doppler technique helps to overcome errors induced by surface slope components in the along-track direction, that is not sufficient.

Error due to an unknown cross-track slope component can be mitigated if its slope is known. Radar interferometry, as an adjunct to a delay-Doppler altimeter, can be used to measure such cross-track surface slopes. The phase-monopulse technique uses this principle to estimate the angle of arrival of reflections from a tilted surface collected through two antennas separated in the cross-track direction of the altimeter (Fig. 13). In a radar altimeter that uses phase-monopulse [28], a scatterer at cross-track distance $\Delta y$ away from nadir precipitates a path length difference $\Delta h$, observable through the cross-channel differential phase. The cross-track phase-monopulse technique can measure the presence of small (mean) cross-track surface slopes. Once measured, the slope data can be applied to recover accurate estimates of the height $h$ of (gently) sloping surfaces. The cross-track phase-monopulse technique complements the delay-Doppler technique, which is an along-track enhancement.

### D2P Airborne Testbed

The first embodiment of the delay-Doppler altimeter combined with a phase-monopulse cross-track receiver is the D2P radar developed at the Johns Hopkins Uniersity Applied Physics Laboratory [29]. The D2P is a coherent airborne radar altimeter that operates from 13.72 to 14.08 GHz (Ku-band). The system transmits a linear FM chirp signal at 5 Watts peak power, with pulse lengths ranging from 0.384 to 3.072 microseconds. The system uses two receiver channels and a pair of antenna arrays, separated by a 14.5 cm baseline, to provide for angle measurements in the cross track direction. The system provides real time display of the delay-Doppler spectrum and cross-track phase of a burst sequence (typically 16 consecutive pulses). The D2P system typically is installed into a P-3 research aircraft. Recent campaigns include flights to Greenland, Svalbard, Antarctica, and over sea ice.

## FUTURE DIRECTIONS

### CryoSat

CryoSat [30] is the first satellite of the European Space Agency's Living Planet Programme to be realized in the framework of the Earth Explorer Opportunity Missions. The mission concept was selected in 1999 with launch originally anticipated in 2004. Unfortunately, the launch (October 2005) failed. A rebuild of CryoSat-2 was approved by ESA, now scheduled for launch in 2009. The Cryosat orbit will have high-inclination (92°) and a long-repeat period (369 days, with a 30-day sub-cycle), designed to provide dense interlocking coverage over the polar regions. Its aim is to study possible climate variability and trends by determining the variations in thickness of the Earth's continental ice sheets and marine sea ice cover.

The Cryosat altimeter will be the first of its kind: SAR/Interferometric Radar ALtimeter (SIRAL), whose advanced modes are patterned after the D2P altimeter [31], and whose flight hardware has extensive Poseidon heritage. Unlike previous radar altimeter missions, Cryosat will downlink all altimetric data. These data will support three modes: conventional, interferometric, and synthetic aperture. The conventional (pulse-limited) mode will be used for open ocean (for calibration and sea surface height

reference purposes) and the central continental ice sheets that are relatively level. The interferometric mode will be used for the more steeply sloping margins of the ice sheets. The synthetic aperture mode will be used primarily over sea ice, where its sharper spatial resolution and better precision will support measurement of the freeboard for floating sea ice. These measurements can be inverted to estimate ice thickness.

### WSOA

The wide-swath ocean altimeter (WSOA) [32] has been promoted by the Jet Propulsion Laboratory as a means to overcome the dominant time/space coverage dilemma that confronts ocean altimetry. The standard altimeter measurement geometry is strictly nadir-viewing: only one sub-satellite height profile is gathered during each pass of the spacecraft. Whereas nadir heights can be very accurate, the surface heights of all regions between nadir tracks remain unobserved, and hence unknown. Many applications would prefer a substantially wider swath of simultaneous height measurements.

Several altimeters have been proposed over the years that would scan the surface below with a set of altimetric beams arrayed orthogonally to the sub-satellite path. The goal is reasonable–to generate a wide swath of height measurements, rather than the single sub-satellite line of data points typically available. However, there are problems with this general approach. The dominant difficulty is that the measurement is based on triangulation, rather than the much more robust (minimum) range measurement of nadir altimetry. Off-nadir triangulation is extremely sensitive to the satellite's roll angle error $\delta\theta$. Height accuracy within a beam-limited paradigm, at an off-nadir measurement angle $\theta$, depends to first order on $h(\tan\,\theta\,\sec^2\,\theta)\delta\theta$, which increases rapidly from zero as the off-nadir angle is increased. In contrast, a pulse-limited nadir altimeter's height measurement accuracy is not degraded in response to small attitude errors at the spacecraft. The height accuracy requirements typical of oceanographic applications of a few cm cannot be met by a single-pass multi-beam or wide swath system given the state-of-the-art of controlling or determining spacecraft (roll) attitude control.

The WSOA concept promises to overcome this roadblock by combining swaths from ascending and descending passes. The accurate nadir heights from one pass will be applied to remove systematic cross-track height errors in the intersecting swath.

### Dual-use altimetry

To date, the two themes of dynamic mesoscale ocean topography and geodesy have remained disjoint. Geodesy requires a non-repeating orbit, whereas traditional oceanographic altimetry, including mesoscale observations, relies on exact-repeat orbits. Recent investigations suggest that the two objectives could be satisfied by one altimeter in a non-repeating orbit, if adequate near-simultaneous ancillary data were available from a more conventional mission such as Jason. The feasibility of dual-use altimetry is a work in progress [35]. If verified, such a mission could be very appealing, since it would attract more potential users (and sponsors), and would require relatively low-cost space-based assets (single frequency, and no WVR, as long as the resolution and precision requirements imposed by geodesy were satisfied). Adoption of this paradigm would require users to think outside of traditional boundaries.

### AltiKa

*AltiKa* [36] differs from other ocean-viewing altimeters in this article, due primarily to its use of Ka-band (35.75 GHz) rather than Ku-band. The first instrument is being built by France for India's Oceansat-3. AltiKa is single-frequency, since at Ka-band the retardation due to the ionosphere is sufficiently small that it does not have to be measured and compensated. However, the $\sim$0.84 cm wavelength is vulnerable to atmospheric moisture; it is predicted that as much as 10% of the data will be compromised by rain. The 33 kg instrument requires an input power of 80 W. The offset-fed reflector antenna is 1 m in diameter, which will have a beamwidth less than half that of its Ku-band counterparts. Several advantages are claimed for the smaller beamwidth, including operation closer to land. On the other hand, the narrower beam implies that the waveform will be more sensitive to spacecraft attitude errors. AltiKa's 500 MHz bandwidth leads to a pulse-limited footprint about 30% smaller than usual. The PRF will be 4 KHz, approximately twice that of most conventional altimeters. The higher PRF implies smaller instrument noise, as long as the returns from adjacent transmissions remain mutually incoherent.

## BIBLIOGRAPHY


1. L.-L. Fu and A. Cazanave, "Satellite Altimetry and the Earth Sciences," Academic Press, 2001, 463 pages.
2. URL/AVISO, "http://www.aviso.oceanobs.com/," July 2003.
3. V. L. Pisacane, "Satellite techniques for determining the geopotential of sea surface elevations," *Journal of Geophysical Research*, vol.**91**, pp. 2365–2371, 1986.
4. M. E. Parke, R. H. Stewart, D. L. Farless, and D. E. Cartwright, "On the choice of orbits for an altimetric satellite to study ocean circulation and tides," *Journal of Geophysical Research*, vol.**92**, pp. 11693–11707, 1987.
5. R. K. Raney, "On orbit selection for ocean altimetry," *IEEE Transactions Geoscience and Remote Sensing*, (to appear), 2003.
6. URL/Geodesy, "http://www.ngdc.noaa.gov/mgg/bathymetry/predicted/explore.HTML," (accessed July 2003).
7. D. T. Sandwell and W. H. F. Smith, "Marine gravity anomaly from Geosat and ERS-1 satellite altimetry," *J. Geophys. Res.*, vol.**102**, pp. 10039–10054, 1997.
8. "Special Sections: Geosat Science and Altimeter Technology," in *Johns Hopkins APL Technical Digest*, Vol**10**, No. 4, 1989.
9. URL/Jason, "http://www-aviso.cls.fr/html/missions/jason/welcome_uk.html," (accessed July 2003).
10. URL/RA-2, "http://envisat.esa.int/instruments/tour-index/ra2/," (accessed July 2003).
11. P. C. Marth, J. R. Jensen, C. C. Kilgus, J. *et al*.," Prelaunch performance of the NASA altimeter for the TOPEX/Poseidon

Project," *IEEE Transactions on Geoscience and Remote Sensing*, vol. **31**, pp. 315–332, 1993.

12. A. R. Zieger, D. W. Hancock, G. S. Hayne, and C. L. Purdy, "NASA radar altimeter for the TOPEX/Poseidon project," *Proceedings of the IEEE*, vol.**79**, pp. 810–826, 1991.
13. S. J. Keihm, M. A. Janssen, and C. S. Ruf, "TOPEX/Poseidon microwave radiometer (TMR) III: Wet troposhperic range correction and pre-launch error budget," *IEEE Transactions on Geoscience and Remote Sensing*, vol.**33**, pp. 147–161, 1995.
14. S. Musman, A. Drew, and B. Douglas, "Ionospheric effects on Geosat altimeter observations," *J. of Geophysical Research*, vol.**95**, pp. 2965–2967, 1990.
15. D. B. Chelton, J. C. Ries, B. J. Haines, *et al.*, "Satellite Altimetry," in *Satellite Altimetry and Earth Sciences, International Geophysics Series*, L.-L. Fu andA. Cazanave, Eds. San Diego: Academic Press, 2001, pp. 1–122.
16. R. K. Moore and C. S. Williams, Jr., "Radar return at near-vertical incidence," *Proceedings of the IRE*, vol. **45**, pp. 228–238, 1957.
17. G. S. Brown, "The average impulse response of a rough surface and its applications," *IEEE Antennas and Propagation*, vol. **25**, pp. 67–74, 1977.
18. W. J. J. Caputi, "Stretch: a time-transformation technique," *IEEE Transactions on Aerospace and Electronic Systems*, vol. **AES-7**, pp. 269–278, 1971.
19. J. L. MacArthur, C. C. Kilgus, C. A. Twigg, and P. V. K. Brown, "Evolution of the satellite radar altimeter," *Johns Hopkins APL Technical Digest*, vol. **10**, pp. 405–413, 1989.
20. E. J. Walsh, "Pulse-to-pulse correlation in satellite radar altimetry," *Radio Science*, vol. **17**, pp. 786–800, 1982.
21. D. B. Chelton, E. J. Walsh, and J. L. MacArthur, "Pulse compression and sea-level tracking in satellite altimetry," *Journal of Atmospheric and Oceanic Technology*, vol. **6**, pp. 407–438, 1989.
22. D. T. Sandwell and W. H. F. Smith, "Bathymetric Estimation," in *Satellite Altimetry and Earth Sciences*, L.-L. Fu andA. Cazenave, Eds. New York: Academic Press, 2001, pp. 441–457.
23. M. M. Yale, D. T. Sandwell, and W. H. F. Smith, "Comparison of along-track resolution of stacked Geosat, ERS-1 and TOPEX satellite altimeters," *J. Geophys. Res.*, vol. **100**, pp. 15117–15127, 1995.
24. W. H. F. Smith and D. T. Sandwell, "Global seafloor topography from satellite altimetry and ship depth soundings," *Science*, vol. **277**, pp. 1956–1961, 1997.
25. R. K. Raney, "The delay Doppler radar altimeter," *IEEE Transactions on Geoscience and Remote Sensing*, vol. **36**, pp. 1578–1588, 1998.
26. R. K. Raney, "Delay compensated Doppler radar altimeter." United States Patent 5, 736, 957, 1998.
27. R. K. Raney, "Radar fundamentals: technical perspective," in *Principles and Applications of Imaging Radar, Manual of Remote Sensing*, F. Henderson andA. Lewis, Eds., 3 ed. New York: Wiley Interscience, 1998, pp. 9–130.
28. J. R. Jensen and R. K. Raney, "Delay Doppler radar altimeter: Better measurement precision," in *Proceedings IEEE Geoscience and Remote Sensing Symposium IGARSS'98*. Seattle, WA, 1998, pp. 2011–2013.
29. J. R. Jensen, "Angle measurement with a phase monopulse radar altimeter," *IEEE Transactions on Antennas and Propagation*, vol. **47**, pp. 715–724, 1999.
30. URL/D2P, "http://fermi.jhuapl.edu/d2p," Johns Hopkins University Applied Physics Laboratory, (accessed July 2003).
31. URL/CryoSat, "http://www.esa.int/export/esaLP/cryosat.html," European Space Agency, (accessed July 2003).
32. R. K. Raney and J. R. Jensen, "An Airborne CryoSat Prototype: The D2P Radar Altimeter," in *Proceedings of the International Geoscience and Remote Sensing Symposium IGARSS02*. Toronto: IEEE, 2002.
33. URL/WSOA, "http://ibib.grdl.noaa.gov/SAT/pubs/Jason2_paper.doc," (accessed July 2003).
34. R. K. Raney and D. L. Porter, "WITTEX: An innovative three-satellite radar altimeter concept," *IEEE Transactions on Geoscience and Remote Sensing*, vol. **39**, pp. 2387–2391, 2001.
35. URL/JHUAPL, "http://fermi.jhuapl.edu/," (accessed July 2003).
36. W. H. F. Smith and R. Scharoo, "ftp://falcon.grdl.noaa.gov/pub/walter/combi_anim.gif," NOAA, (accessed July 2003).

R. KEITH RANEY
Johns Hopkins University,
Laurel, MD